Exploring the possibilities of increasing energy density and efficiency in rechargeable batteries

Download this complimentary article collection

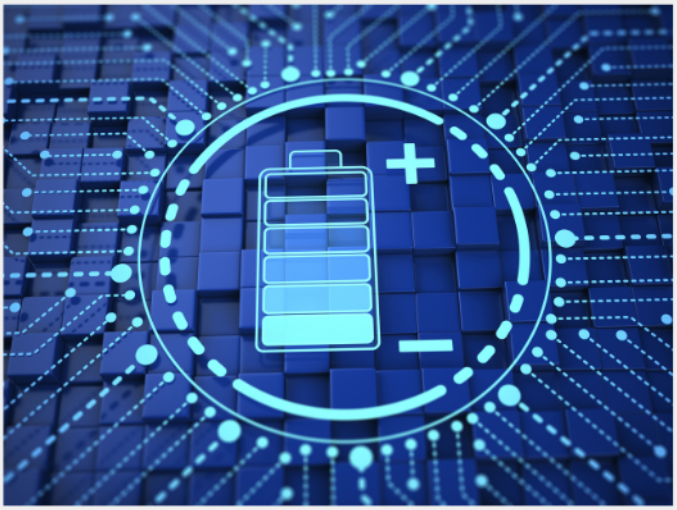

The exponential rise in the need for better, more efficient power sources has sparked an incredible amount of research into batteries. A primary focus of research has been increasing the energy density of batteries, as it allows for lighter, more portable storage of energy. Lithium-ion batteries, for example, have a much higher energy density than conventional lead-acid batteries and can be used for various purposes, such as in electric vehicles.

This article collection provides a comprehensive list of references for new methods and technologies for increasing the energy density of batteries.

Metrohm

WILEY

ADVANCED FUNCTIONAL MATERIALS
www.afm-journal.de

A Self-Powered Body Motion Sensing Network Integrated with Multiple Triboelectric Fabrics for Biometric Gait Recognition and Auxiliary Rehabilitation Training

Chuanhui Wei, Renwei Cheng, Chuan Ning, Xuyang Wei, Xiao Peng, Tianmei Lv, Feifan Sheng, Kai Dong, and Zhong Lin Wang**

Gait analysis provides a convenient strategy for the diagnosis and rehabilitation assessment of diseases of skeletal, muscular, and neurological systems. However, challenges remain in current gait recognition methods due to the drawbacks of complex systems, high cost, affecting natural gait, and one-size-fits-all model. Here, a highly integrated gait recognition system composed of a self-powered multi-point body motion sensing network (SMN) based on full textile structure is demonstrated. By combining of newly developed energy harvesting technology of triboelectric nanogenerator (TENG) and traditional textile manufacturing process, SMN not only ensures high pressure response sensitivity up to 1.5 V kPa^{-1}, but also is endowed with several good properties, such as full flexibility, excellent breathability (165 mm s^{-1}), and good moisture permeability (318 g m^{-2} h^{-1}). By using machine learning to analyze periodic signals and dynamic parameters of limbs swing, the gait recognition system exhibits a high accuracy of 96.7% of five pathological gaits. In addition, a customizable auxiliary rehabilitation exercise system that monitors the extent of the patient's rehabilitation exercise is developed to observe the patient's condition and instruct timely recovery training. The machine learning-assisted SMN can provide a feasible solution for disease diagnosis and personalized rehabilitation of the patients.

1. Introduction

With the increasing prevalence of infectious diseases and the growing trend of population aging, the current mainstream hospital or clinic centralized, therapy-oriented, and even one-size-fits-all medical model is facing huge challenges, due to the lack of continuous vital signs monitoring, real-time health management and maintenance, and long-term treatment plan implementation.[1,2] Fortunately, the rapid development of information technology, the popularization of intelligent terminals, the advancement of sensor technology,[3] and the improvement of Internet infrastructure have provided soil and nutrients for the vigorous growth of Internet medical and wearable medical electronics.[4–6]

Gait, as one of the most common behavioral characteristics, requires the coordination and common role of the nervous system, muscle system, and skeletal system. Each individual's gait exhibits different dynamic characteristics due to the diversity of length of the leg bone, muscle strength, center of gravity, motor nerve sensitivity, and even external trauma. It also depends on a variety of factors, such as age, habitus, gender and diseases.[7–9] The main features of gait contain numerous biomechanical and kinematic parameters, which can reflect a series of physiological, physical, nervous states, and even psychological problems.[10,11] The impact of many diseases on human body is displayed in the form of deformity gait, and the classification of abnormal gait is significant to reveal the key aspects and influencing factors of gait abnormalities, which will assist clinical diagnosis, guide rehabilitation training and enforce efficacy assessment.[12–15] With the integration of measurement technology and wearable electronic technology,

C. Wei, R. Cheng, C. Ning, X. Peng, T. Lv, F. Sheng, K. Dong, Z. L. Wang
CAS Center for Excellence in Nanoscience
Beijing Key Laboratory of Micro-Nano Energy and Sensor
Beijing Institute of Nanoenergy and Nanosystems
Chinese Academy of Sciences
Beijing 101400, P. R. China
E-mail: dongkai@binn.cas.cn; zhong.wang@mse.gatech.edu

C. Wei, R. Cheng, X. Peng, K. Dong
School of Nanoscience and Technology
University of Chinese Academy of Sciences
Beijing 100049, P. R. China

The ORCID identification number(s) for the author(s) of this article can be found under https://doi.org/10.1002/adfm.202303562.

C. Ning
College of Materials Science and Engineering
Key Laboratory of Material Processing and Mold (Ministry of Education)
Henan Key Laboratory of Advanced Nylon Materials and Application
Zhengzhou University
Zhengzhou 450001, P. R. China

X. Wei
Department of Software Engineering
Harbin University of Science and Technology
Rongcheng 264300, P. R. China

Z. L. Wang
School of Material Science and Engineering
Georgia Institute of Technology
Atlanta, GA 30332-0245, USA

DOI: 10.1002/adfm.202303562

gait analysis has gradually shifted from qualitative research to various parts of sports and dynamic quantitative research. It is worth noting that relying solely on doctors for the diagnosis of gait disorders makes the diagnosis subjective and greatly increases the lag of medical recovery. The combination of artificial intelligence technology and wearable gait sensors makes medical diagnosis and treatment more accurate, data-based and scientific.[16–19] This will also provide data support for the design and development of rehabilitation aids.

According to the placement position and working mechanism, the current commonly used gait recognition methods can be divided into two categories: fixed monitoring and mobile monitoring. Far infrared cameras and depth cameras equipped with motion capture systems are fixed on the wall or brackets, which is based on the optical principle of capturing the body's joint points and thus analyzing their kinetic parameters.[20–22] However, there are still several bottlenecks in the access of public, due to high costs, restricted monitoring space, huge data volumes, and potential security issue. Direct measurement of acceleration of limb and flexion angles using wearable accelerometers and goniometers is one of the most common methods in medical and sports monitoring.[20,23] However, rigid instruments based on silicon-based integrated circuits are difficult to fit the human body, affecting natural gait and causing physiological and psychological uncomfortable feelings. Textiles have the attributes of multi-level and multi-scale structures, good flexibility, and wearing comfort, which is an excellent carrier of gait monitoring sensors.[24] Smart textiles that integrate traditional textile processes and advanced flexible sensor technology are used in the field of gait recognition, which not only retains the natural flexibility and breathability, but also achieves gait monitoring on-site and in real time. This perfectly fits the needs of clinical diagnosis and rehabilitation assistance in diversified and portable medical models, and realizes the inductiveness of medical monitoring.[25,26] Triboelectric nanogenerator (TENG) is a newly developed energy harvesting and self-powered sensing technology based on the coupling effect of contact electrification and electrostatic induction,[27] which is widely used in the field of motion tracking,[28] human–machine interaction,[29] and medical monitoring.[1,30–33] For health monitoring, triboelectric textile sensors have been widely demonstrated to be effective for gait analysis.[1,34] For example, Sun et al. developed a triboelectric textile sensor integrated on the insole, which prepared conductive fabric electrons by applying MXene ink on the fabric.[10] With the assistance of machine learning algorithms, the triboelectric insole can accurately monitor the gait patterns of people. Wang et al. reported a triboelectric textile sensor based on conductive fiber and TPU membrane, which can be sewn on the socks.[11] The triboelectric socks are used to distinguish normal gait with Parkinson's gait, issue alarms about falling, and preciously judge the identity of five users by combining neural network as well. The strategy that sewing the triboelectric textiles on the socks or carpets has been widely demonstrated, which is effective to monitor pace pressure for gait analysis. However, this strategy is difficult to analyze limb oscillation and rotation. As an important parameter in gait analysis, periodic signal and dynamic parameters of limbs swing and coordination are often overlooked. In addition, many textile-based sensors still use opaque materials as the packaging layer, or tape for adhesion, which may cause skin inflammation.[32,35–37] Full-textile sensors need to be constructed to improve the breathability and flexibility of wearable devices,[38] which will reduce the wearing discomfort and psychological barriers for patients.

Here, a self-powered multi-point body motion sensing network (SMN) based on the structure of the whole textile is presented for biometric gait recognition and auxiliary rehabilitation training. SMN is implemented through conventional knitting processes and emerging digital embroidery craft. Compared to the common plane fabric pressure sensor, the knitted double-ribbed structure sensing node using knitting technology has higher pressure linear sensitivity. The sensing node has a high linear fitting slope (1.5 V kPa^{-1}) under the external load force is smaller than 2 kPa, while the plain fabric sensor has a response sensitivity of 0.02 V kPa^{-1}. Subsequently, SMN is integrated into garments to obtain gait signals from patients with deformed gait. A set of support vector machine (SVM) algorithm was used to process the sensing information. By extracting the time sequence and dynamic parameters of the limb swinging, the gait recognition system can effectively recognize and classify five deformed gait patterns with a high accuracy (96.7%). In addition, an auxiliary rehabilitation training system in which patients can perform appropriate training as planned is developed. Moreover, SMN has all the nature of daily garments, with excellent breathability (165 mm s^{-1}), moisture permeability (318 g m^{-2} h^{-1}), and wash resistance (remain above 85% of the initial performance after 12 h of water washing). Based on the above results, we predict that the highly integrated gait recognition system consists of SMN, a set of machine learning algorithm and a real-time human–machine interface will provide a new avenue for intelligent personalized healthcare.

2. Result and Discussion

2.1. Overview of the Smart Gait Recognition and Rehabilitation System

As shown in **Figure 1**a, a self-powered multi-point body motion sensing network (SMN) based on the whole textile structure is proposed for biometric gait recognition and auxiliary rehabilitation training. The sensing network is connected by multiple full textile-based sensing nodes in several parts of the body, which enables effective multi-point monitoring of gait information throughout the body. In the network, the sensing node is vertically stacked by a top cotton fabric, a 3D double-ribbed knitted fabric (KF), a conductive fabric (CF), and a bottom cotton fabric. Cotton fabrics are used as packaging layers due to the advantages of light, soft, breathable and easy to integrate. Ag fiber is used as the core wire of the composite yarn because of its superior conductivity, flexibility and stretchability, while multiple polyethylene fibers are used as sheath layers. Subsequently, the composite yarn was knitted into a 3D double-ribbed structure. Compared with common plane fabric, the 3D double-ribbed structure has a wider response range and higher sensitivity to the pressure. This is because more three-dimensional structure causes a broader range of contact area for more effective contact electrification effect. The surface of the conductive

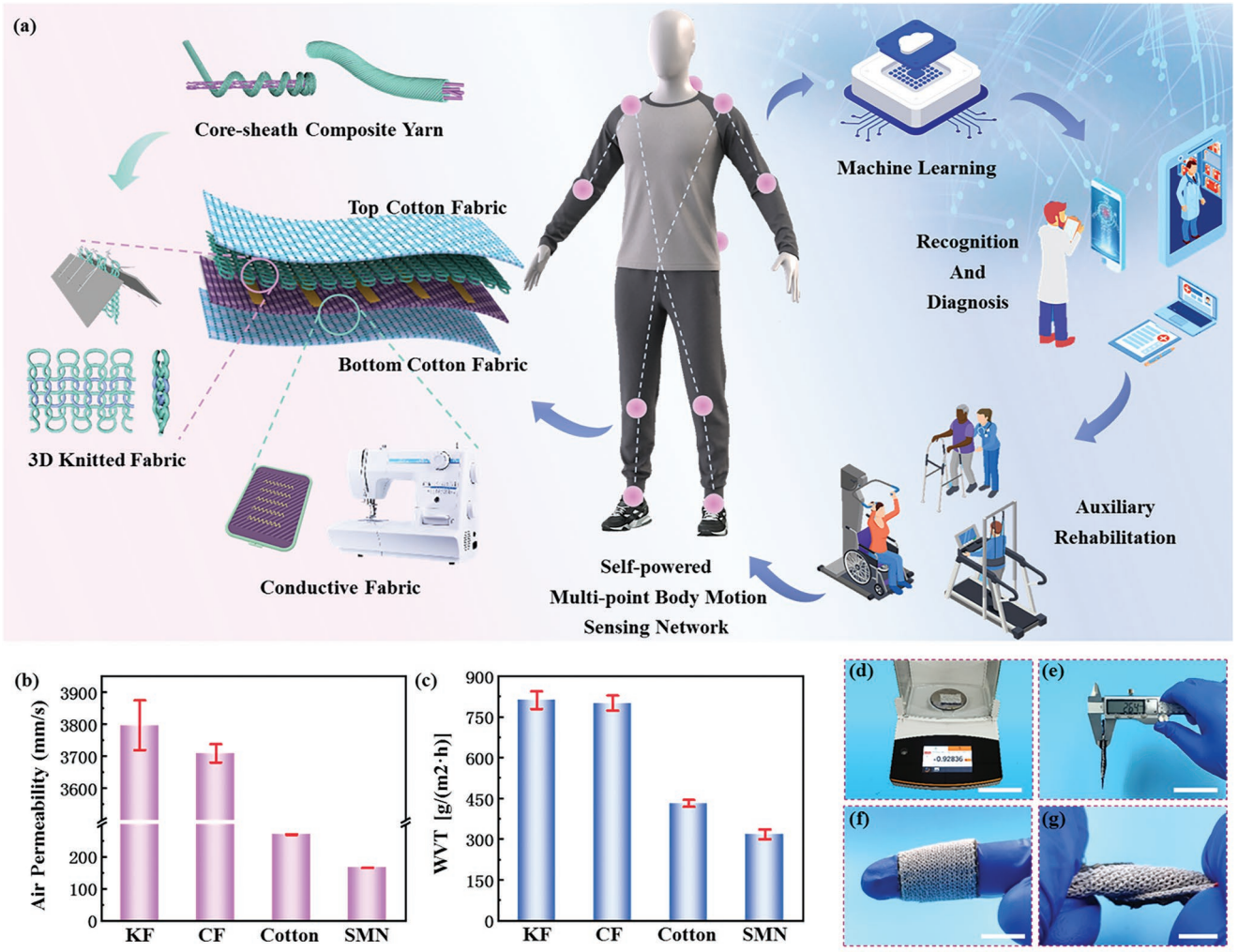

Figure 1. Schematics illustration of highly integrated gait recognition system. a) Structural design of textile-based self-powered multi-point body motion sensing network (SMN) and schematics diagram of highly integrated gait recognition system. b) Air permeability and c) moisture permeability of different fabrics and SMN, respectively. Demonstration of d) lightness, e) thinness, and f,g) flexibility of SMN. The scale bars in (d–g) are 10, 5, 1, and 1 cm, respectively.

fabric uses the digital embroidery process to prepare the spacers to support the textile sensor. Considering that commercial cotton and PE fibers are widely used in clothing, and Ag fiber has been widely proven to have good antibacterial properties, SMN is used directly as a skin contact interface integrated on clothing for body motion monitor. Thanks to the principle of TENG, SMN integrated into the everyday outfits generates multi-channel dynamic signals during walking spontaneously. The multi-channel parallel electrical signals are fed into the machine learning algorithms to identify five common deformed gait patterns. In addition, a real-time human–machine interaction platform is also developed for biometric gait recognition and auxiliary rehabilitation training.

For textile-based electronic devices directly exposed to skin, breathability is fundamental and vital for improving skin comfort, which mainly includes the performance of air permeability, moisture permeability, insulation and warmth. The air permeability of SMN and commercial clothing was compared under different pressure differences (Figure S1, Supporting Information). As the pressure difference increases from 50 to 200 Pa, the air permeability of SMN increases linearly and consistently outperforms the commercial clothing. Under the pressure difference of 50 Pa and an area of 20 cm^2, the air permeability of the 3D knitted fabric and conductive fabric is as high as 3796 and 3708 mm s^{-1}, respectively (Figure 1b). This is extremely high performance for fabric. Despite the breathability of SMN is limited to 165 mm s^{-1} due to the encapsulated cotton fabric, it is still higher than most commercial apparel and is sufficient to meet the comfort needs of daily wear without causing any inflammation. The air permeability of SMN can be further improved by changing the encapsulation layer to meet different service conditions. In addition to air permeability, moisture permeability and weight are also important factors affecting comfort. The moisture permeability affects the volatilization of sweat secreted on the surface of the skin, which affects the most intuitive feeling of humanity on textile comfort. The moisture permeability performance exhibits a similar phenomenon (Figure 1c). All the four samples show high moisture

permeability, and the indexes of the knitted fabric and the conductive fabric are 811.3 and 800.4 g m^{-2} h^{-1}, respectively. The moisture permeability performance of SMN was 318 g m^{-2} h^{-1}, which is sufficient to meet the comfort needs. SMN is light (61.9 mg cm^{-2}, Figure 1d), while Figure 1e demonstrates that a sensing node with two cotton encapsulation layers has a thin thickness of 2.64 mm. Light quality and thin thickness also prove that SMN is very suitable for wearable sensors. SMN can be easily wrapped on a finger (Figure 1f), reversing 360° without destroying its own structure (Figure 1g), which shows that its good flexibility can fully meet the requirements of fit our skin. Based on the above experimental results, SMN has the advantages of outstanding breathability, lightweight, and excellent flexibility, which ensures that SMN can be seamlessly integrated into garments for imperceptible gait monitoring.

2.2. Core-Sheath Composite Yarn

Figure 2a,b shows the schematic diagram and work principle diagram of a custom-made scalable elastic wrapping device for continuous preparing core-sheath composite yarns, respectively. The core-sheath composite yarn is fabricated through wrapping the multi-strand PE yarn over the surface of the conductive Ag yarn. Ag yarn is selected as the core wire because it has excellent conductivity, stretching and antibacterial properties. Note that, during the preparation process of the composite yarn, the sheath yarn is subject to the complex stress effect of centrifugal, tensile, twisting and frictional force. Complex stress scenarios mainly come from the rotation and swing of yarns, which requires the sheath yarn to possess a certain self-adaptive ability. Multi-stranded yarns have a flexible and

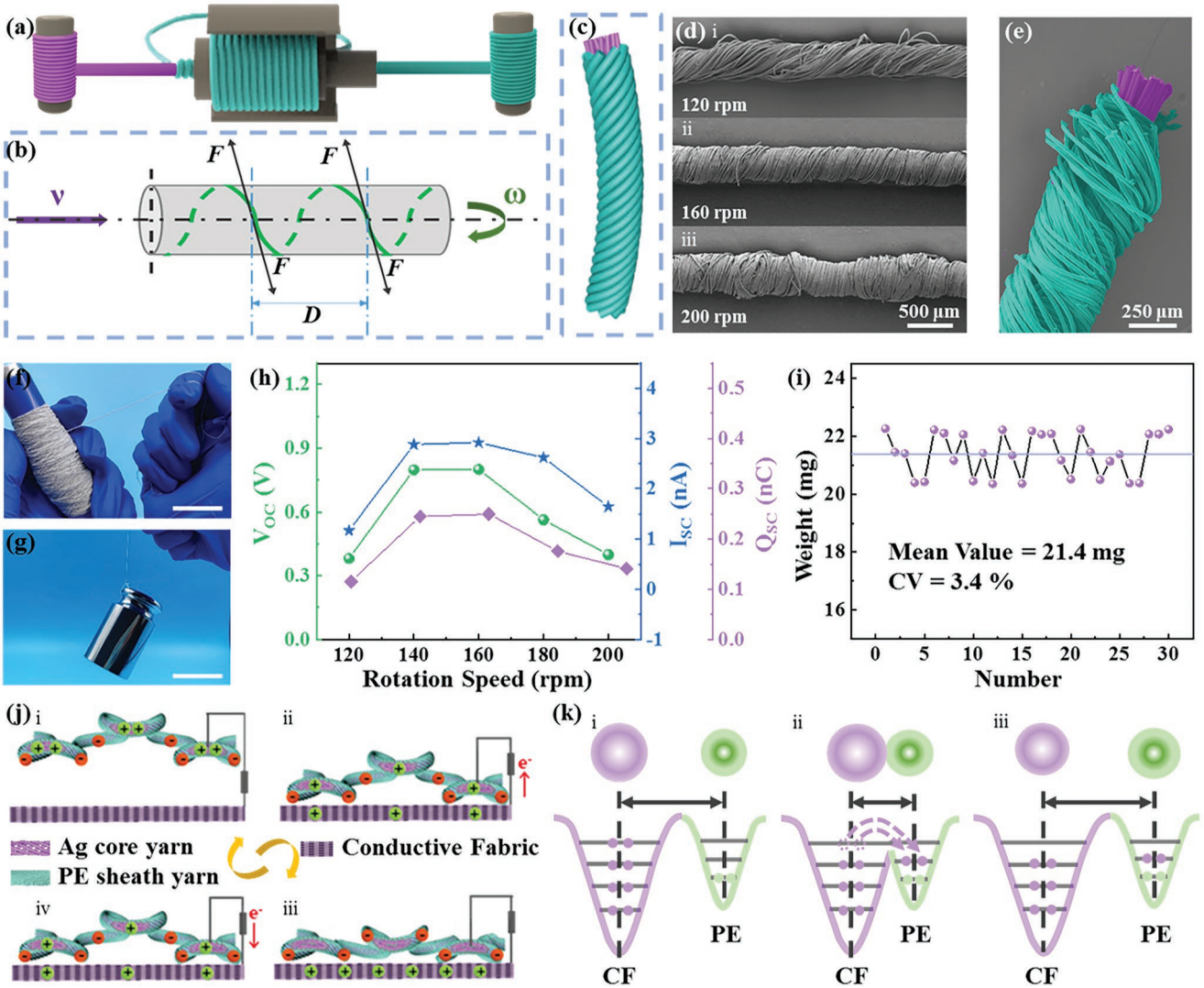

Figure 2. Properties of Ag-PE core-sheath composite yarn and working mechanism of SMN. a,b) Schematic diagram of the manufacturing process and parameters of Ag-PE core-sheath composite yarn. c) Schematic of composite yarn. d) SEM images of composite yarns fabricated under different wrapping speeds. e) SEM image of the endpoint of composite yarn. f) Demonstration of mass-produced yarns. g) Strength proof picture of composite yarn. The weight of the heavy object is 500 g. h) Electrical output characteristics of a single 5 cm long yarn prepared at different wrapping speeds, including V_{OC}, I_{SC}, and Q_{SC}. i) Weight and uniformity of composite yarn by a quantitative test method. j) Working mechanism of SMN. k) Atomic-scale-electron-cloud potential-well model to describe the contact electrification between conductive fabric (CF) and PE sheath yarn.

variable cross-section shape to adapt to different stress scenes. To realize the uniform preparation and smooth surface morphology of the composite yarn, the spontaneous adaptation and deformation ability of multiple yarns is crucial. The naked core wires and undesirable knots caused by equipment instability can be eliminated to a certain extent through this spontaneous adjustment. Multiple PE yarns are selected as the raw yarn rather than single-ply yarns to prepare a composite yarn, so that there is a higher fault tolerance rate during the preparation process. As shown in Figure S4 (Supporting Information), Ag-PE composite yarns with different diameters were easily prepared due to self-adaptive ability, while Ag-PTFE composite yarns were discarded after extensive efforts. In addition, compared with single-stranded PTFE yarn, the multi-stranded PE yarn can effectively increase the friction between the core and sheath yarn, making the composite yarn serviceable for knitting. Furthermore, to ensure that the fabric sensor has a large tensile strength and stable sensing performance, PE yarns instead of other low-modulus yarns are selected as sheath yarn (Figure 2c). The preparation process is mainly divided into three parts, feeding the raw yarn, rotating wrap, and receiving composite yarn. Each part has its corresponding motor-driven mechanical components. In the production process, the surface morphology of the core-spun yarn can be adjusted by adjusting the feeding speed of the core wire and the rotation speed of the sheath yarn (Figure 2b).

Figure 2d and Figure S2 (Supporting Information) show the optical microscope and SEM images of the core-sheath composite yarn under different rotation speed of the sheath yarn (120, 160, and 200 rpm). The low rotation speed of the sheath yarn causes the core to be incompletely wrapped, which is highly susceptible to short circuits (120 rpm, Figure 2d). The excessive rotation speed leads to cross-linking of multiple PE yarns, which further result in knotting (200 rpm, Figure 2d). By adjusting these wrapping parameters, the most suitable processing parameters were obtained, in which conditions, the composite yarn revealed good uniformity with no short-circuit and no thick knots. In this work, the core yarn conveying speed is 74 mm min^{-1} and the rotation speed of sheath yarn is 160 rpm.

In addition to experimental testing, dynamic theory in the process of elastic packets is also quantified. In detail, the geometrical parameters during yarn wrapping should satisfy Equation (1):

$$\tan\theta = \frac{\mathrm{v}}{2\pi \mathrm{w}(\mathrm{r}+\mathrm{d})} \tag{1}$$

When the core is just completely wrapped by the sheath yarn and no knots appear, the geometric parameters should satisfy Equation (2):

$$\sin\theta = \frac{\mathrm{D}}{2\pi(\mathrm{r}+d)} \tag{2}$$

In the above equations, θ is the angle between the sheath yarn and the direction perpendicular to the core, v is the feeding speed of the core, w is the wrapping speed of the sheath, r is the radius of the core, d is the radius of the sheath yarn in the vertical direction to the composite yarn, and D represents the diameter of the sheath in the parallel direction to the composite yarn.

The parameter K is defined by Equation (3):

$$\mathrm{K} = 2\pi(\mathrm{r}+\mathrm{d}) \tag{3}$$

By combining geometric Equation (4):

$$1+\cot^2\theta = \csc^2\theta \tag{4}$$

The critical ratio of w/v when the core yarn is just covered by the sheath can be calculated as:

$$\frac{\omega}{\mathrm{v}} = \frac{\mathrm{D}}{\mathrm{K}\sqrt{\mathrm{D}^2-\mathrm{K}^2}} \tag{5}$$

When the w/v value is less than the critical value, the core wire cannot be completely covered; when the w/v value is greater than the critical value, the sheath yarn is knotted. Since the cross-section of multi-stranded sheath yarn is self-adaptable according to dynamics, the shape of the cross-section is slightly deformed compared with the rules. This leads to the rotation speed and linear speed of the experimental measurement mildly different from the theoretical value, but their dynamic process still has high similarity.

For the core-sheath composite yarn, the degree of coverage of the sheath layer determines the mechanical performance and electrical performance of the yarn. The stress-strain curve demonstrates that the composite yarn, which is just tightly wrapped but without knots, also displays the best mechanical properties (Figure S3, Supporting Information). Figure 2g intuitively shows the mechanical properties of the yarn with a core-sheath structure. A single yarn can easily lift a weight of 500 g without any damage. In Figure 2e, the apparent core-sheath structure of the yarn can be clearly seen in the SEM picture of the end of a composite yarn, and the Ag core yarn is evenly wrapped by the sheath yarn (Figure 2f). The composite yarn continuously produced by the elastic wrapping machine show a uniform diameter and a smooth surface, and this process is scalable, industrial and extended. To test the uniformity in the procession, 30 pieces of core-sheath yarns of 30 cm were weighed and the calculated average was 21.4 mg with a coefficient of variation of 3.4% (Figure 2i). This indicates that the prepared yarn has the potential for large-scale homogenization preparation, which also provides a guarantee of stable performance for the commercial application of textile-based triboelectric sensing network in the future. Compared with other rotational speeds, the single composite yarn at a rotational speed of 160 rpm also show the highest electrical output, with V_{OC}, I_{SC}, and Q_{SC} of 0.8 V, 2.9 nA, and 0.2 nC, respectively (Figure 2h). The working principle of TENG is based on the coupling effect of contact electrification and electrostatic induction. Therefore, the reasons that affect the output of composite yarn can be simply attributed to two points: the effective contact electrification area and thickness of the tribo-layer. In general, the larger the effective contact electrification area, the more transferred charges, and the higher the electrical output of the composite yarn. The thicker the tribo-layer, the less charge is induced on the core

wire, and the lower the output of the composite yarn. The wrapping area of the PE yarn is small when the rotation speed is very low, the smaller effective electrification area of the composite yarn results in a decrease in the output area and further decreases the electrical output performance. As the rotational speed increases, the core wire is wrapped more tightly by the sheath yarn, the effective contact area increases, and the output gradually increases. When the rotational speed is too high, the electrical performance is degraded for two reasons. The first point is that the intertwined nodes are formed between the PE yarns, leading to the inadequate contact of the dielectric layer with the tribo-layer and further a reduced transferring charge. The second point is that the high wrapping speed increases the thickness of the PE yarn layer, which reduces the induced charge on the core wire. Both of these points cause a reduction in electrical output performance when the wrapping speed exceed. The effect of different thicknesses of sheath yarns on the morphology and output of the composite yarn was also analyzed in detail. Ag-PE composite yarns with uniform morphology and gradually increasing diameter were prepared by increasing the number of wrapping (Figures S5 and S6a, Supporting Information). As the thickness increased, the stretchability of the composite yarn gradually became worse, the amount of induced charge on the core decreased, and the electrical output decreased, so single-wrapped Ag-PE composite yarns were used (Figures S6b and S7, Supporting Information). The excellent mechanical performance of composite yarn ensures the feasibility of the knitting process, the preparation of large-scale and uniformity guarantees the huge prospects of industrial production, and the high electrical output performance warrants the high sensitivity and response ability of the sensor.

As shown in Figure 1a, the knitting process is chosen to woven the core-sheath composite yarn into a double ribbed fabric, which has outstanding breathability, flexibility, pressure response ability. Figure 2j illustrates the working mechanism of a sensing node in SMN in the short-circuit state. The self-powered sensing node works in the dual-electrode vertical contact separation mode, one electrode is the Ag core wire of the composite yarn, and the other electrode is conductive fabric. The space between the double-rib knitted fabric and the conductive fabric is prepared through the emerging digital embroidery process, which can maintain the patterned shape with high precision. As shown in **Figure 3**a and Figure S8 (Supporting Information), the digital embroidery process is proven to achieve the perfect restoration of patterns and shapes on the surface of fabric.

The surface of the PE yarn is filled with negative charges due to contact-electrification, and an equal number of positive charges flows back and forth between the two electrodes, thereby forming an alternating electric current. When the conductive fabric and the double-ribbed knitted fabric are separated, due to the negative charge exists on the surface of the PE sheath yarn, the positive charge will be attracted to the Ag wire of the core layer (Figure 2j-i). As shown in Figure 2j-ii,iii, free electrons will flow from the Ag core yarn to the conductive fabric as the double-rib knitted fabric contacts the conductive fabric. Due to the three-dimensional fluffy structure, SMN with the double-ribbed knitted fabric displays a more diverse pressure response than the membrane or plain weave fabric. For a more accurate understanding, the process by which the 3D knitted fabric being compressed is shown in Figure S10 (Supporting Information). When the external mechanical stimulation is relatively small, the inner side of the rib structure just contact the conductive fabric. When the external pressure stimulation increases, the inner ribbed yarn is in touch first with conductive fabric, and the outer ribbed yarn is squeezed and subsequently contacted with conductive fabric. Under different external stimuli, SMN shows varying degrees of compression-rebound response, which is unique to the common plane fabric sensor.

The electron-cloud-potential-well model between the metal and the dielectric can perfectly explain the physical origin of the contact electrification [25]. For this work, the model explains the electron transport mechanism between the PE sheath yarn of double-rib fabric and the conductive fabric at the atomic scale (Figure 2k). The model states that contact electrification between materials is due to the overlapping of electron cloud between the two materials when they are in contact. Figure 2k-i illustrates that before the two materials reach atomic-level contact, the electron clouds of the two atoms remain separated. Their potential wells confine their respective electrons to specific regions, preventing the electrons from escaping freely. When external stress is applied, the electron clouds of the two atoms will overlap. The initial symmetric potential well will become an asymmetric potential well, and because the strong electron cloud overlap reduces the energy level barrier between the two. As a result, atoms with strong electronegativity obtained the opponent's electrons (Figure 2k-ii), which caused the phenomenon of electronic transfer. When the external force is removed (Figure 2k-iii), the transferred electrons obtained by PE with strong electronegativity are bound to become static electrons, thereby showing a negative characteristic. While the contact and separation of materials occurs on the macroscopic scale, the transfer and chain of electrons also occurs on the atomic scale accordingly.

2.3. Output Performance of SMN

Digital embroidery is a product of combing traditional Chinese craftsmanship and modern digital technology, which can create various decorative patterns and structure on the fabric. As shown in Figure 1a and Figure 3a, the digital embroidery process was used to prepare the spacer between the double-ribbed knitted fabric and conductive fabric. To prove that the embroidery process is applicable to different patterns, four different patterns are utilized, which shows a very high reduction accuracy (Figure S8, Supporting Information). Figure 3b shows that under the same area, different numbers of parallel intervals as spacers have an impact on the electrical output performance. When the six rectangular intervals are adopted, SMN gets the highest electrical output performance. When the number of intervals is less, the complete separation between the knitted fabric and the sliver fabric cannot be achieved. Conversely, it results in incomplete contact between the two. There are optimal parameters to achieve optimal electrical output performance. As illustration in Figure 3c, different

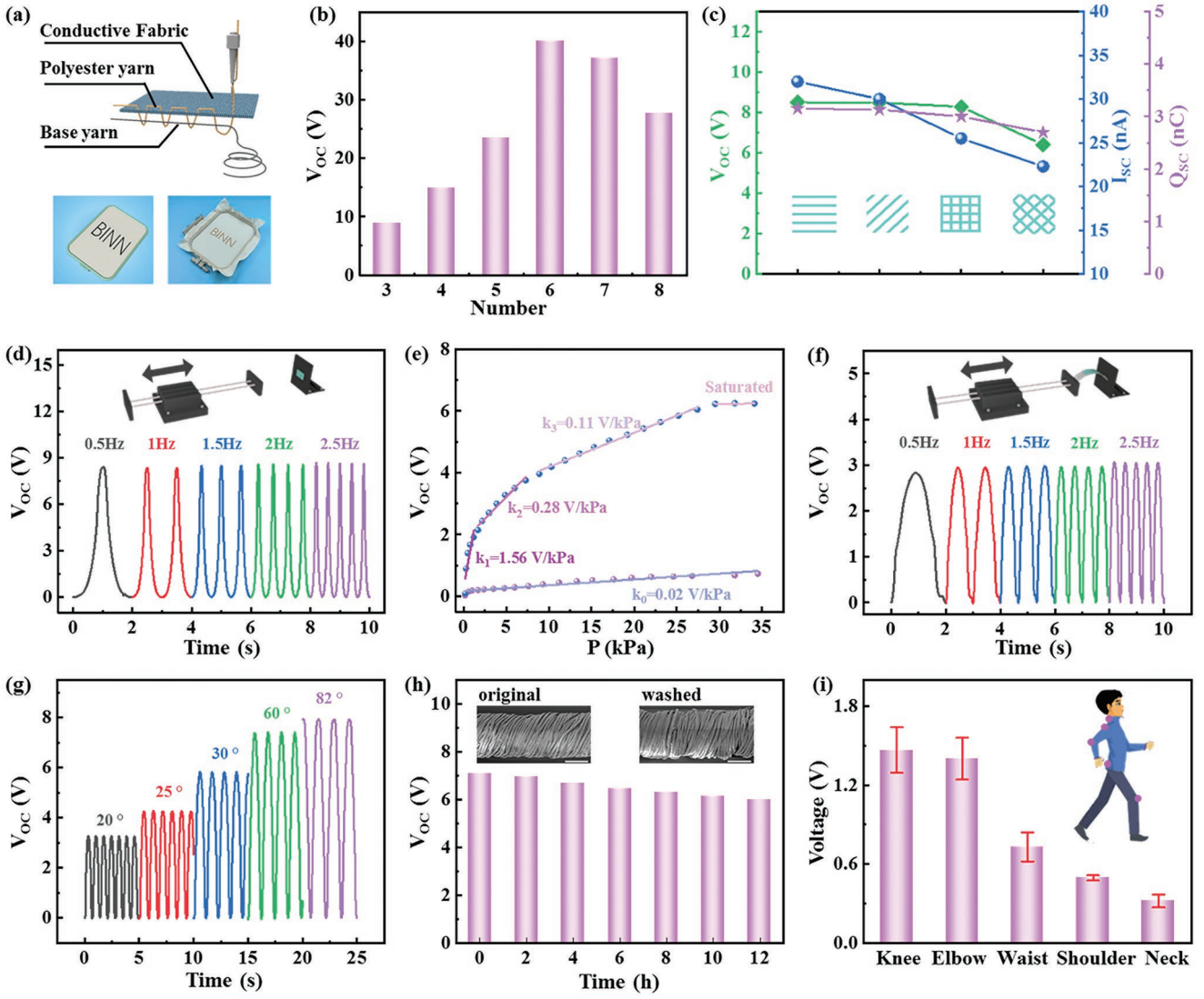

Figure 3. Preparation process and electrical properties of SMN. a) Schematic diagram of patterned preparation of spacers of SMN. b,c) Electrical properties of SMN with different spacer numbers and patterns. d) Frequency response output performance of SMN under vertical stress. e) Pressure response curve of SMN and plain fabric pressure sensor under vertical stress. f,g) Frequency and angle response output performance of SMN under bending condition. h) The washability test of SMN. The insets are the SEM images of the surface morphology before and after water washing, both scale bars are 200 µm. i) Sensing performance of sensing nodes integrated into different body parts. The inset is a schematic diagram of the placement sites of the nodes on the human body.

patterns are designed as the supporting structure, which will also affect the sensing properties. When the angle of the spacer and the boundary was 0°, the electrical properties were better than those with an angle of 45°. When only parallel spacers are present, electrical performance is better than those with cross-pattern intervals. The angle and pattern affect the contact area of knitted fabric and conductive fabric, which leads to different performance of SMN.

The electrical output of the SMN was quantified under different external mechanical stimulation. Considering that when a person walks, the frequency and magnitude of the mechanical pressure applied to the clothes are irregular, so it is necessary to analyze the sensor performance of SMN under different circumstances. Figure 3d illustrates that in the vertical contact-separation mode, the peak of open-circuit voltage (V_{OC}) remains essentially constant as the frequency increases from 0.5 to 2.5 Hz. Since there is no dynamic charge transfer process in the open circuit state, the voltage is only affected by the charge density and separation distance, independent of frequency. Thanks to the sensitivity of the 3D knitted structure to pressure, the pressure response sensitivity of SMN is much better than that of plain fabric pressure sensors (Figure 3e). The pressure response curve of SMN is divided into four regions, namely high, medium, low pressure response regions and saturation region. The highest response sensitivity is 1.56 V kPa^{-1} under pressure below 2 kPa. When the pressure is between 2 and 8 kPa, the response sensitivity decreases to 0.28 V kPa^{-1}. When the pressure is between 8 and 28 kPa, the response

sensitivity is 0.11 V kPa^{-1}. When the pressure is higher than 28 kPa, the sensing performance of SMN shows a saturation state. Compared to SMN, the pressure sensor of plain weave fabric exhibits a lower pressure response throughout the entire testing range, with a sensitivity of only 0.02 V kPa^{-1}. The SMN exhibits excellent stability and long-term robustness of electrical properties, with no significant output degradation at over 10 000 cycles (Figure S17, Supporting Information). Besides, the response time is an important parameter to reflect the sensitivity of the sensor. Due to the increase of the contact-separation frequency, the time of each working cycle is shortened, and the response time and recovery time of SMN are reduced accordingly from 331 and 357 ms at the initial 1 Hz to 100 ms and 110 ms at 4 Hz respectively (Figure S18, Supporting Information). The sensing network nodes integrated into joint parts withstand the forces not only from the vertical direction, but also from the bending direction. As shown in Figure 3f, the electrical output performance of SMN upon bending was also tested. The V_{OC} of SMN remained stable when the bending frequency was changed from 0.5 to 2.5 Hz. This is because the bending frequency does not affect the surface charge density and the separation distance. However, with the bending angle increases, the effective contact and separation area increases. And the distance between the two becomes larger, which leads to the enhancement of the electrical performance (Figure 3g). In addition, SMN exhibits a good washing resistance. As shown in Figure 3h, the V_{OC} of SMN was tested after washing every two hours, which still remain above 85% of the initial performance after 12 h of water washing. Insets are the SEM images of the knitting fabric before and after washing. It can be seen that the surface does not change significantly, which proves that the SMN has excellent mechanical property and washing resistance. Multiple sensing nodes were integrated into different sites of the garments to build the SMN, including knee, elbow, waist, shoulder and neck. Each sensing node can effectively monitor external pressure, which verifies the feasibility for monitoring gait information and performing gait recognition and auxiliary rehabilitation training. It can be proved in Figure 3i that when the sensing nodes were placed on the wearer's knee and elbow, SMN exhibits the best electrical output performance and sensing property. Therefore, in later subsequent testing and demonstration, the elbows and knees were chosen as sensing nodes for gait monitoring.

2.4. Smart Gait Recognition System

Deformed gait can be caused by a variety of neurological and musculoskeletal diseases, which leads to nerve degeneration, muscle atrophy and knee dislocation. A smart gait recognition system consisting of the SMN, machine learning algorithms, and human–computer interface was applied in the discrimination of deformed gait and the rehabilitation guidance for patients. As shown in **Figure 4**a,b, the SMN with multiple sensing nodes was integrated on the elbows and knees, respectively. When the human body walks, along with the bending and swinging of the limbs, the SMN generates corresponding multi-channel electrical signals, which are used as the source of machine learning data analytics. Abnormally pathological gaits can be detected and differentiated, such as Parkinson's gait (PG), scissors gait (SG), mopping gait (MG), gluteus maximums gait (GG), and cross-threshold gait (CG). The five common pathological gaits are often caused by nervous system retardation, muscle atrophy, or external injury. Each deformed gait shows its special posture and limb orientation, which results in the specific electrical signal waveform for each deformed gait (Figure 4c). To achieve excellent gait signal analysis and accurate classification functions, machine learning algorithms are introduced into the gait sensing system. Support Vector Machine (SVM) is a linear classification algorithm with perfect mathematical theory, which is a typical supervised learning algorithm.[39] For the above five gaits, a multiple SVM algorithm with a Gaussian kernel function is constructed to achieve accurate classification.

The machine learning model based on the SVM algorithm is divided into two parts. The first part is the training of the model, that is, supervised learning. The second part is the testing of the model, that is, real-time recognition of gaits. For a machine learning algorithm, feature values are independently observable properties or characteristics of an object or pattern. The selection of a feature value has a significant impact on the construction of the algorithm and the effectiveness of the recognition. The peaks and troughs of the signals are typical, readily obtained, and effective data features for linear classification. Therefore, the peaks and troughs of the signals from the four channels (CP1, CT1, CP2, CT2, CP3, CT3, CP4, CT4) are selected as the feature values. Due to the different movement times of limbs during walking for different patients, it is necessary to select the periodic feature as the feature value of training. The time when channel 1 obtains the peak is selected as the reference time, that is, the relative zero point. The mathematical relative difference between the time of the other seven peaks or valleys and the reference time are taken as the feature value, which can greatly enhance the accuracy of training. The way that using seven relative time lags (T1, T2, T3, T4, T5, T6, T7) instead of eight absolute times not only greatly improves the temporal correlation of the limbs, but also reduces the training load of the algorithm. In summary, for each of the 300 signals of the five gait patterns, 15 eigenvalues were extracted. The data formed a data matrix of 300 rows and 15 columns, and a 300-dimensional label vector with five elements was constructed. Each 15-dimensional row vector corresponds to a label, and the label is used as a supervised learning to realize the linear classification of the data source. The various algorithms and verification methods of machine learning were adopted, which strongly verify the effectiveness of the selection of eigenvalue selection based on time domain signals. For SVM algorithms with four different kernel functions and two other linear classification algorithms, the accuracy of linear classification validated using the 20% leave-out method before and after the introduction of timing features is compared. As shown in Figure 4 and Figure S20 (Supporting Information), the introduction of timing features is crucial for improving the accuracy of linear classification. The gait recognition system based on SMN and SVM algorithm exhibits a classification accuracy of up to 96.7%, and the performance is very robust (Figure 4e). For the SVM algorithm of other kernel functions and other linear classification algorithms, all the accuracy of recognition exceeds 80% (Figure 4d). In order to increase

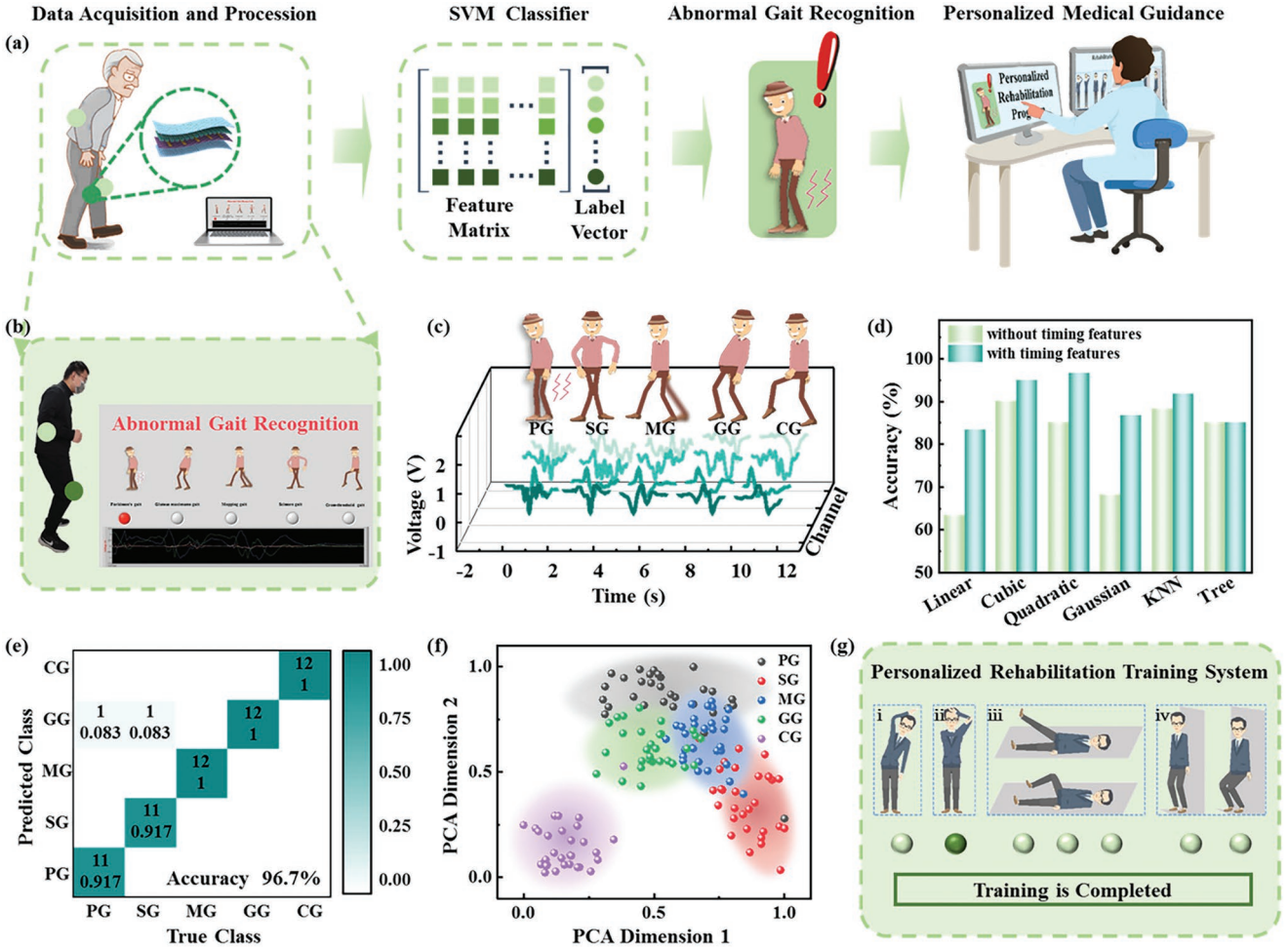

Figure 4. High integrated gait monitoring system based on SMN. a) Schematic diagram of real-time gait monitoring system for biometric gait recognition and auxiliary rehabilitation training. b) The real scene and human–machine interface of the deformed gait recognition system. c) Maps and typical multi-channel sensing signals of five deformed gaits, including Parkinson's gait (PG), scissors gait (SG), mopping gait (MG), gluteus maximus gait (GG), and cross-threshold gait (CG). d) Classification accuracy contrast of different machine learning algorithms validated using the 20% leave-out method for five deformed gaits with and without timing signals. e) Confusion matrix of the SVM algorithm using 20% leave-out method for five gaits. f) Principal component analysis (PCA) of five typical gait signals. g) Human–machine interface of personalized auxiliary rehabilitation training system.

the amount of data in the training set and avoid overfitting, fivefold cross-validation is used as another validation method (Figures S21 and S22, Supporting Information). Among the two validation methods used, the SVM algorithm based on peak and timing features showed high linear classification accuracy. In addition, the parallel coordinates plot of the feature values of the five gaits show that the five gaits have a clear clustering effect, especially the peak has a clear contribution in the classification (Figure S23, Supporting Information).

To more intuitively show the limb discrepancies and signal differences of the five gaits, the method of principal component analysis (PCA) was applied. For high-dimensional non-linear data, PCA can map samples to linear non-related variables through a simple orthogonal transformation. In addition, PCA can reduce the gait data of high dimensions to two-dimensional space. As seen in Figure 4f, the dimensionality reduction outputs of the five gaits exhibit good clustering characteristics. This suggests that the application of machine-learning schemes for medical diagnosis is promising.

2.5. Customized Medical Rehabilitation Platform

The purpose of identifying and diagnosing diseases through gait data is to achieve early prevention, treatment and rehabilitation training for patients. In the future smart medical system, besides disease monitoring, medical rehabilitation will also have a huge demand and a broad market prospect. Rehabilitation training for patients with abnormal gait often requires the assistance and supervision of external medical devices. The SMN is also expected to be used in medical auxiliary rehabilitation systems, which can develop individualized and targeted rehabilitation programs for patients according to gait recognition results and other medical metrics. A human–computer interaction platform for patients to rehabilitate is briefly demonstrated in Figure 4g and Video S2 (Supporting Information). Take Parkinson's gait as an example, the system presets four types of training, namely shoulder twist, side bend, lie flexion straight leg and knee flexion. Through classification, counting, and standard judgment of the action, doctors can obtain and

supervise the patient's recovery situation. When the number of trainings is not enough and the amplitude is too small, which cannot effectively stimulate the nerve and muscle system, the training action is considered invalid. Only when the amplitude and number of rehabilitation movements of the patient reach the standard, the system will indicate "Training is completed". As discussed above, SMN provides a suitable and promising solution for the construction of a smart medical auxiliary rehabilitation training platform.

3. Conclusions

In summary, a textile-based self-powered multi-point body motion sensing network (SMN) is developed for gait recognition and auxiliary rehabilitation exercises, which can be seamlessly and senselessly integrated into the garments. The sensing network is prepared through traditional knitting and emerging digital embroidery process, which not only provides excellent pressure response and short response time, but also maintains outstanding breathability (165 mm s^{-1}), moisture permeability (318.0 g m^{-2} h^{-1}), washing resistance and high stability over 10 000 working cycles. Unlike other wearable gait sensors placed under the feet, the sensing nodes of SMN are placed at the joints to analyze the amplitude and timing of the limbs. Combining the multi-channel sensor data with machine learning algorithms, a gait recognition system achieved high recognition accuracy (96.7%) of five deformed gait patterns, including Parkinson's gait, scissors gait, mopping gait, gluteus maximums gait, and cross-threshold gait. In addition, an auxiliary rehabilitation system is also built to realize the role of intelligent medical treatment, which can determine the intensity and standard degree of training. As discussed above, this research provides an efficient and comfortable new solution for biometric gait recognition and auxiliary rehabilitation training, demonstrating the broad development and application prospects of smart textile-based sensing network in the field of intelligent medical.

4. Experimental Section

Materials: Commercially produced Ag yarn (200D) and multi-strand polyethylene (PE) yarn (200D) were purchased from Dongguan Shengxin Special Cord Co., Ltd. The cotton fabric was provided by Zhejiang Kaida Fabric Co., Ltd. The conductive fabric was produced by Anhui Aijia Radiation Protection Technology Co., Ltd.

Fabrication of Ag-PE Core-Sheath Composite Yarn: The production equipment that could continuously produce core-sheath composite yarns on a large scale was manufactured by Tianjin Tianyuan Precision Machinery Co., Ltd. The core wire conveying speed was 74 mm min^{-1} and the sheath rotation speed was 160 rpm.

Fabrication of SMN: The knitting process was used to prepare the double-ribbed knitted fabric. The WILCOM software was used to design, and a novel digital embroidery machine (NV180, Brother) was used to produce the patterned spacers of SMN. Cotton fabric was used as an encapsulation layer using a sewing process.

Characterization and Measurement: The air permeability was tested at 50 Pa pressure difference with a test area of 20 cm^2. Moisture permeability was tested according to GB/T 12704.1-2009 standard. A system based on a programmable electrostatic meter (Keithley 6514) and a multi-channel acquisition card (NI-6356) was used to test the electrical output performance including V_{OC}, I_{SC} and Q_{SC}. A linear motor (LinMot E1100) was used to apply cyclic contact separation and bending for SMN. Preprocessing and linear classification of gait data in machine learning by programming with MATLAB software. The human–machine interaction interface of the smart gait recognition system and rehabilitation exercise platform was achieved based on LabVIEW software. Real-time linear classification was implemented by calling the pre-trained program in MATLAB software through the LabVIEW software. The COSMOL software was used to simulate the spatial potential distribution.

Supporting Information

Supporting Information is available from the Wiley Online Library or from the author.

Acknowledgements

C.W., R.C., and C.N. contributed equally to this work. The authors are grateful for the support received from Natural Science Foundation of the Beijing Municipality (Grant Nos. L222037 and 2212052), National Natural Science Foundation of China (Grant No. 22109012), the National Key R & D Project from the Ministry of Science and Technology (Grant No. 2021YFA1201601), and the Fundamental Research Funds for the Central Universities (Grant No. E1E46805). No formal approval for the experiments involving human volunteers was required. The volunteers took part following informed consent.

Conflict of Interest

The authors declare no conflict of interest.

Data Availability Statement

The data that support the findings of this study are available from the corresponding author upon reasonable request.

Keywords

gait recognition, machine learning, rehabilitation training, self-powered sensing, triboelectric textiles

Received: March 30, 2023
Revised: April 19, 2023
Published online:

[1] W. Wang, J. Pang, J. Su, F. Li, Q. Li, X. Wang, J. Wang, B. Ibarlucea, X. Liu, Y. Li, W. Zhou, K. Wang, Q. Han, L. Liu, R. Zang, M. H. Rümmeli, Y. Li, H. Liu, H. Hu, G. Cuniberti, *InfoMat* **2021**, *4*, 12262.
[2] R. Jain, A. S. Lakhnot, K. Bhimani, S. Sharma, V. Mahajani, R. A. Panchal, M. Kamble, F. Han, C. Wang, N. Koratkar, *Nat. Rev. Mater.* **2022**, *7*, 736.
[3] M. Wu, X. Wang, Y. Xia, Y. Zhu, S. Zhu, C. Jia, W. Guo, Q. Li, Z. Yan, *Nano Energy* **2022**, *95*, 106967.
[4] Z. Lai, J. Xu, C. R. Bowen, S. Zhou, *Joule* **2022**, *6*, 1501.
[5] Y. Bonnassieux, C. J. Brabec, Y. Cao, T. B. Carmichael, M. L. Chabinyc, K.-T. Cheng, G. Cho, A. Chung, C. L. Cobb,

A. Distler, H.-J. Egelhaaf, G. Grau, X. Guo, G. Haghiashtiani, T.-C. Huang, M. M. Hussain, B. Iniguez, T.-M. Lee, L. Li, Y. Ma, D. Ma, M. C. McAlpine, T. N. Ng, R. Österbacka, S. N. Patel, J. Peng, H. Peng, J. Rivnay, L. Shao, D. Steingart, et al, *Flex. Print. Electron.* **2021**, *6*, 023001.
[6] X. Zhao, H. Askari, J. Chen, *Joule* **2021**, *5*, 1391.
[7] S. Studenski, S. Perera, K. Patel, C. Rosano, K. Faulkner, M. Inzitari, J. Brach, J. Chandler, P. Cawthon, E. B. Connor, M. Nevitt, M. Visser, S. Kritchevsky, S. Badinelli, T. Harris, A. B. Newman, J. Cauley, L. Ferrucci, J. Guralnik, *JAMA, J. Am. Med. Assoc.* **2011**, *305*, 50.
[8] Z. Liu, S. Sarkar, *IEEE Trans Pattern Anal Mach Intell* **2006**, *28*, 863.
[9] D. Tao, X. Li, X. Wu, S. J. Maybank, *IEEE Trans Pattern Anal Mach Intell* **2007**, *29*, 1700.
[10] P. Sun, N. Cai, X. Zhong, X. Zhao, L. Zhang, S. Jiang, *Nano Energy* **2021**, *89*, 106492.
[11] Q. Zhang, T. Jin, J. Cai, L. Xu, T. He, T. Wang, Y. Tian, L. Li, Y. Peng, C. Lee, *Adv. Sci.* **2022**, *9*, 2103694.
[12] M. Cesari, *JAMA, J. Am. Med. Assoc.* **2011**, *305*, 93.
[13] L. Wang, T. Tan, H. Ning, W. Hu, *IEEE Trans Pattern Anal Mach Intell* **2003**, *25*, 1505.
[14] Y. Matsuzawa, M. Konishi, E. Akiyama, H. Suzuki, N. Nakayama, M. Kiyokuni, S. Sumita, T. Ebina, M. Kosuge, K. Hibi, K. Tsukahara, N. Iwahashi, M. Endo, N. Maejima, K. Saka, K. Hashiba, K. Okada, M. Taguri, S. Morita, S. Sugiyama, H. Ogawa, H. Sashika, S. Umemura, K. Kimura, *J Am Coll Cardiol* **2013**, *61*, 1964.
[15] A. Fasano, A. E. Lang, *Lancet Neurol.* **2015**, *14*, 675.
[16] R. Wu, S. Seo, L. Ma, J. Bae, T. Kim, *Nano-Micro Lett.* **2022**, *14*, 139.
[17] F. Wen, Z. Sun, T. He, Q. Shi, M. Zhu, Z. Zhang, L. Li, T. Zhang, C. Lee, *Adv. Sci.* **2020**, *7*, 2000261.
[18] Y. Jiang, J. An, F. Liang, G. Zuo, J. Yi, C. Ning, H. Zhang, K. Dong, Z. L. Wang, *Nano Res.* **2022**, *15*, 8389.
[19] Q. Shi, Z. Zhang, Y. Yang, X. Shan, B. Salam, C. Lee, *ACS Nano* **2021**, *15*, 18312.
[20] K. Jun, S. Lee, D. W. Lee, M. S. Kim, *IEEE Access* **2021**, *9*, 161576.
[21] Y. X. Wang, X. Zhang, Y. R. Shen, B. W. Du, G. R. Zhao, L. C. C. Lizhen, H. K. Wen, *IEEE Trans Pattern Anal Mach Intell* **2022**, *44*, 3436.
[22] A. Mirelman, P. Bonato, R. Camicioli, T. D. Ellis, N. Giladi, J. L. Hamilton, C. J. Hass, J. M. Hausdorff, E. Pelosin, Q. J. Almeida, *Lancet Neurol.* **2019**, *18*, 697.
[23] R. Mason, L. T. Pearson, G. Barry, F. Young, O. Lennon, A. Godfrey, S. Stuart, *Sports Med* **2023**, *53*, 241.
[24] B. Wang, A. Facchetti, *Adv. Mater.* **2019**, *31*, 1901408.
[25] M. Chen, P. Li, R. Wang, Y. Xiang, Z. Huang, Q. Yu, M. He, J. Liu, J. Wang, M. Su, M. Zhang, A. Jian, J. Ouyang, C. Zhang, J. Li, M. Dong, S. Zeng, J. Wu, P. Hong, C. Hou, N. Zhou, D. Zhang, H. Zhou, G. Tao, *Adv. Mater.* **2022**, *34*, 2200985.
[26] H. Yao, Z. Wang, Y. Wu, Y. Zhang, K. Miao, M. Cui, T. Ao, J. Zhang, D. Ban, H. Zheng, *Adv. Funct. Mater.* **2022**, *32*, 2112155.
[27] Z. L. Wang, A. C. Wang, *Mater. Today* **2019**, *30*, 34.
[28] C. Jia, Y. Xia, Y. Zhu, M. Wu, S. Zhu, X. Wang, *Adv. Funct. Mater.* **2022**, *32*, 2201292.
[29] L. Wang, W. Liu, Z. Yan, F. Wang, X. Wang, *Adv. Funct. Mater.* **2020**, *31*, 2007221.
[30] Q. Zhang, C. Xin, F. Shen, Y. Gong, Y. Zi, H. Guo, Z. Li, Y. Peng, Q. Zhang, Z. L. Wang, *Energy Environ. Sci.* **2022**, *15*, 3688.
[31] C. Wu, A. C. Wang, W. Ding, H. Guo, Z. L. Wang, *Adv. Energy Mater.* **2019**, *9*, 1802906.
[32] X. Peng, K. Dong, Z. Y. Wu, J. Wang, Z. L. Wang, *J. Mater. Sci.* **2021**, *56*, 16765.
[33] Z. Yan, L. Wang, Y. Xia, R. Qiu, W. Liu, M. Wu, Y. Zhu, S. Zhu, C. Jia, M. Zhu, R. Cao, Z. Li, X. Wang, *Adv. Funct. Mater.* **2021**, *31*, 2100709.
[34] G. Chen, X. Xiao, X. Zhao, T. Tat, M. Bick, J. Chen, *Chem. Rev.* **2021**, *122*, 3259.
[35] S. Choi, S. I. Han, D. Jung, H. J. Hwang, C. Lim, S. Bae, O. K. Park, C. M. Tschabrunn, M. Lee, S. Y. Bae, J. W. Yu, J. H. Ryu, S. W. Lee, K. Park, P. M. Kang, W. B. Lee, R. Nezafat, T. Hyeon, D. H. Kim, *Nat. Nanotechnol.* **2018**, *13*, 1048.
[36] Z. Ma, Q. Huang, Q. Xu, Q. Zhuang, X. Zhao, Y. Yang, H. Qiu, Z. Yang, C. Wang, Y. Chai, Z. Zheng, *Nat. Mater.* **2021**, *20*, 859.
[37] X. Peng, K. Dong, Y. Zhang, L. Wang, C. Wei, T. Lv, Z. L. Wang, Z. Wu, *Adv. Funct. Mater.* **2022**, *32*, 2112241.
[38] K. Dong, Y. Hu, J. Yang, S. W. Kim, W. Hu, Z. L. Wang, *MRS Bull.* **2021**, *46*, 512.
[39] W. S. Noble, *Nat. Biotechnol.* **2006**, *24*, 1565.